

ARTICLE

Flexible nanohybrid substrates utilizing gold nanocubes/nano mica platelets with 3D lightning-rod effect for highly efficient bacterial biosensors based on surface-enhanced Raman scattering

Received 00th January 20xx,
Accepted 00th January 20xx

DOI: 10.1039/x0xx00000x

Yan-Feng Chen,^a Ming-Chang Lu,^a Chia-Jung Lee^b and Chih-Wei Chiu^{*a}

In this study, gold nanocubes (AuNCs) were quickly synthesized using the seed-mediated growth method and reduced onto the surface of two-dimensional (2D) delaminated nano mica platelets (NMPs), enabling the development of AuNCs/NMPs nanohybrids with a 3D lightning-rod effect. First, the growth-solution amount can be changed to easily adjust the AuNCs average-particle size within a range of 30–70 nm. The use of the cationic surfactant cetyltrimethylammonium chloride as a protective agent allowed the surface of AuNCs and nanohybrids to be positively charged. Positively charged nanohybrid surfaces presented a good adsorption effect for detecting molecules with negative charges on the surface. Additionally, the NMP surfaces were rich in ionic charges and provided a large specific surface area for stabilizing the growth of AuNCs. Delaminated AuNCs/NMPs nanohybrids can generate a 3D hotspot effect through self-assembly to enhance the Raman signal. Surface-enhanced Raman scattering (SERS) is highly sensitive in detecting adenine biomolecules. Its limit of detection (LOD) and Raman enhancement factor reached 10^{-9} M and 3.6×10^8 , respectively. Excellent reproducibility was obtained owing to the relatively regular arrangement of AuNC particles, and the relative standard deviation (RSD) was 10.7%. Finally, the surface of NMPs was modified by adding the hydrophilic [polymer poly\(oxethylene\)-diamine \(POE2000\)](#) and amphiphilic [polymer-PIB-POE-PIB copolymer](#) at different weight ratios. The adjustment of the surface hydrophilicity and hydrophobicity of AuNCs/NMPs nanohybrids led to better adsorption and selectivity for bacteria. AuNCs/POE/NMPs and AuNCs/PIB-POE-PIB/NMPs were further applied to the SERS detection of hydrophilic *Staphylococcus aureus* and hydrophobic *Escherichia coli*, respectively. The SERS-detection results suggest that the LOD of hydrophilic *Staphylococcus aureus* and hydrophobic *Escherichia coli* reached 92 CFU/mL and 1.6×10^2 CFU/mL, respectively. The AuNCs/POE/NMPs and AuNCs/PIB-POE-PIB/NMPs nanohybrids had different hydrophilic–hydrophobic affinities, which greatly improved the selectivity and sensitivity for detecting bacteria with different hydrophilicity and hydrophobicity. Therefore, fast, highly selective, and highly sensitive SERS biological-detection results were obtained.

Introduction

In recent years, noble metallic nanoparticles have enabled the development of nanotechnology due to their unique optical and electrical properties.^{1–3} In particular, gold nanoparticles possess extremely high chemical stability and biocompatibility^{4,5} and have been widely used in applications related to biosensing technology.^{6–8} Optical properties primarily depend on the localized surface plasmon resonance (LSPR) of particles.⁹ When nanoparticles are excited by light irradiation, their surface electrons produce collective and coherent oscillations. These oscillations are localized near tiny metal structures, and their frequencies vary depending on the material, shape, particle

size, and surrounding medium.^{10,11} Therefore, the synthesis of gold nanoparticles of various shapes and the control of particle sizes has been attracting increasing attention. Gold nanocubes (AuNCs) have strong local electric-field intensity at their tips and a wide range of LSPR tunability.¹² Owing to their flat surfaces, these particles can self-assemble into large-scale orderly nanostructures that are stacked in a specific order; thus, they can potentially be used for surface-enhanced Raman scattering (SERS).^{13–15} AuNCs are typically prepared using seed growth;¹⁶ the synthesis process has limitations such as a long preparation time and cumbersome steps. Therefore, this study uses a seed-mediated method to prepare AuNCs,¹⁷ making the AuNC-preparation process simpler and faster. In this method, the size of the AuNCs is mainly controlled by adjusting the amount of gold seed solution added;¹⁸ however, this causes the loss of excessive gold solution. Based on cost considerations, we chose to change the amount of intermediate added and confirmed the tunability of the particle size, providing another solution for controlling the particle size of AuNCs.

Two-dimensional (2D) nanomaterials, as the known thinnest materials, have uniform shapes and high surface-area-to-

^a Department of Materials Science and Engineering, National Taiwan University of Science and Technology, Taipei 10607, Taiwan.

^b Ph.D. Program in Clinical Drug Development of Herbal Medicine, College of Pharmacy, Taipei Medical University, Taipei 11031, Taiwan.

*Corresponding author. E-mail: cwchiu@mail.ntust.edu.tw; Tel.: +886-2-2737-6521

†Electronic Supplementary Information (ESI) available: additional information on synthesis, characteristics, and performance of AuNCs/NMPs nanohybrid material. See DOI: 10.1039/x0xx00000x

volume ratios.^{19–21} In our previous work, synthetic fluorinated mica (Mica) was prepared using a one-step delamination method to form nano mica nanoplatelets (NMPs),^{22,23} which were used as a substrate for the stable growth of metallic nanoparticles.²⁴ Owing to the large number of ionic charges on the surfaces of delaminated NMPs, the particles can produce a 3D hotspot effect through self-assembly to enhance the Raman signal.²⁵ In addition, layered nanoclay comprising silicon-oxygen bonds has a hydrophilic surface owing to the polar structure of the silicon-oxygen bonds. Its affinity to hydrophilic molecules can be increased through the polar interactions on the surface;²⁶ however, the surface is incompatible with and cannot interact with hydrophobic molecules. The amphiphilic polymer designed in this study was used to modify the surface of NMPs; thus, the hydrophilic NMPs can form hydrophobic organic clay. Therefore, the surface hydrophilicity and hydrophobicity of nanohybrids can be controlled, the AuNCs can grow stably, and the adsorption capacity for the analyte molecules can be increased through polar adsorption,²⁷ forming selective and highly sensitive SERS substrates.

Bacteria are among the main groups of organisms, and their bacterial types are typically identified via Gram staining classification.²⁸ Staining divides bacteria into two major categories based on the different compositions and structures on the bacterial-cell wall: Gram-positive bacteria and Gram-negative bacteria.^{29,30} Generally, teichoic acid, as a component in the cell wall, is unique to Gram-positive bacteria, which leads to more negative charges and hydrophilicity on the surface of positive bacteria.³¹ In addition, Gram-negative bacteria do not contain teichoic acid, but contain components such as an outer membrane, lipoprotein, and lipopolysaccharide (LPS). Therefore, the surface of negative bacteria is more hydrophobic.³² This study uses *Staphylococcus aureus* (*S. aureus*) and *Escherichia coli* (*E. coli*) as representatives of positive and negative bacteria, respectively, both of which are widespread in nature and harmful to the human body. As report suggests that SERS spectral analysis can extract highly specific vibrational information from individual bacteria,^{33–35} reducing the required analysis time. Additionally, it enables strain identification for different bacteria, allowing SERS detection technology to recognize various bacterial species through spectral fingerprints.^{363–396} The SERS-detection technology is used to identify different bacterial species through spectral fingerprints.^{33,34} The SERS substrate designed in this study can capture *S. aureus* and *E. coli* through physical adsorption to increase the Raman signal intensity, thereby enabling the rapid detection of biomolecules or bacteria without fluorescent labeling.

This study developed a novel type of organic/inorganic nanohybrid. This type of nanohybrid can select polymeric surfactants with different hydrophilic–hydrophobic properties and adjust the surface energy of nanomaterials, thereby increasing the selective adsorption of different bacterial species. In our previous work, well-established nanohybrids comprising noble metallic nanoparticles and 2D materials were used as the basis of the SERS substrate and exhibited extremely high sensitivity for detecting single molecules and

biomolecules.^{40375–42397} In this study, an improved seed-mediated method was used to prepare AuNCs, and the lightning-rod effect formed by AuNCs was employed to increase the SERS signal intensity for biomolecules. In addition, this study proposes the application of AuNCs in SERS bacterial detection for the first time, confirming the feasibility of AuNCs in bacterial molecular detection. Next, 2D delaminated NMPs were used as the substrate to stably reduce AuNCs to form AuNCs/NMPs nanohybrids with a 3D lightning-rod effect. Finally, the hydrophilic polymer poly(oxyethylene)-diamine (POE2000) and amphiphilic polymer PIB–POE–PIB were applied to adjust the surface energy of nanohybrids at different weight ratios to selectively detect hydrophilic *S. aureus* and hydrophobic *E. coli*. Additionally, bacteria were captured through physical adsorption, thereby enhancing the signal of SERS spectra. The limit intensity of detection under different concentrations of bacterial liquid was also explored. This method provides a rapid and highly sensitive detection of biomolecules and achieves selectivity for sensing hydrophilic and hydrophobic bacteria.

Experimental section

Materials

Tetrachloroauric acid (99.9% purity), sodium borohydride (NaBH_4 , 98% purity), and N-Hexadecyltrimethylammonium chloride (CTAC) were purchased from Echo Chemical Co. (Taiwan). Sodium bromide (NaBr , 99.5% purity) was purchased from Showa Chemical Industry Co., Ltd. (Japan). Ascorbic acid (99% purity) was purchased from Acros Organics Corp. Synthetic fluorinated mica (Mica) (SOMASIF ME-100), which comprised Si (26.5 wt%), Mg (15.6 wt%), F (8.8 wt%), Na (4.1 wt%), Al (0.2 wt%), and Fe (0.1 wt%), was purchased from CO-OP Chemical Co. (Japan). Polyisobutylene-g-succinic anhydride (PIB–SA, Mw = 1,335) was purchased from Chevron Corporation (USA). Poly(oxyethylene)-diamine (POE–diamine, Mw = 2,000) was purchased from Huntsman Chemical Co. (USA). Adenine (purity 99.9%) was purchased from Sigma–Aldrich Chemical Co. *S. aureus* strain (BCRC 10781, ATCC 25923) was obtained from the Bioresource Collection and Research Center (Hsinchu, Taiwan). *E. coli* strain (BL 21, ATCC 25922) was obtained from the American Type Culture Collection (USA).

Preparation of gold nanocube (AuNC) solution

AuNCs were synthesized using an improved seed-mediated method.⁴³⁹³⁸ First, the gold seed solution was prepared. HAuCl_4 (0.01 M, 0.25 mL) and CTAC (0.1 M, 9.75 mL) were thoroughly mixed, and NaBH_4 (0.02 M, 0.45 mL) was added slowly in an ice bath and stirred vigorously for 1–2 s. At this time, the solution turned brown. It was maintained at a temperature of 30 °C for 1 h to ensure the stable generation of gold seed solution. Then, two samples were chosen and labeled as Growth 1 (G1) and Growth 2 (G2) to prepare the growth solution. CTAC (0.1 M, 10 mL), NaBr (0.01 M, 0.01 mL), and HAuCl_4 (0.01 M, 0.25 mL) were added to both bottles of growth solution. Subsequently, ascorbic acid (0.04 M, 0.09 mL) was slowly added dropwise as the reducing agent, and the solution gradually turned from light yellow to colorless. Next, we added 0.065 mL of gold seed

solution to G1 and continued to stir until the solution turned light pink (approximately 10 s). Then, we immediately added 0.3 mL of G1 into G2 and mixed them thoroughly for approximately 2 s. Finally, we let the G2 solution stand at 25 °C for 5 min to form AuNCs. The color of the solution turned dark red. The resulting AuNC solution was centrifuged at 6,000 rpm for 30 min and washed repeatedly with deionized (DI) water at least three times to remove excess CTAC.

Preparation of AuNC/NMP nanohybrids

A schematic of the NMP synthesis is shown in **Fig. S1, ESI**. NMPs were prepared according to a previously reported procedure.^{44,39} First, Mica (1.0 g, 1wt%) was swelled at 80 °C for 1 h. Subsequently, the swollen Mica was added to the acidified delamination agent T403AEO, followed by 5 h of continuous stirring.²³ Finally, NaOH was extracted and added to the delaminated clay solution, purified several times with ethanol solution, and then redispersed in DI water to form a 1 wt% NMP solution. **Fig. S2, ESI** shows the X-ray diffraction (XRD) detection in the case of clay delamination. The original Mica's 2θ angle was 7°, and its d-spacing was 12.6 Å. When a delaminating agent was added to perform cation exchange with the clay and polymerize layered clay, the van der Waals forces between the clay layers were destroyed, leading to the delamination of the clay. At this time, the absence of any diffraction peaks in XRD detection indicates that Mica delaminated into monolithic NMPs. Using atomic force microscopy, we observed that the thickness of Mica was approximately 20.01 nm owing to the layer-by-layer stacking (**Fig. S3, ESI**). **Fig. S4, ESI** shows that the thickness of monolithic NMPs was approximately 2.25 nm. The variations in thickness also confirmed the good delamination and dispersion effect. After different weight ratios of NMPs and HAuCl₄ (0.01 M, 0.25 mL) were stirred in CTAC (0.1 M, 10 mL) for 1 hour, NaBr (0.01 M, 0.03 mL) and the reducing agent, ascorbic acid (0.04 M, 0.09 mL) were added. Then, the gold seed solution (0.065 mL) was added to the G1 solution (CTAC: 0.1 M, 10 mL; NaBr: 0.01 M, 0.01 mL; HAuCl₄: 0.01 M, 0.25 mL; ascorbic acid: 0.04 M, 0.09 mL). They were stirred until the solution turned light pink (approximately 10 s). We immediately added 0.3 mL of G1 into the HAuCl₄/NMP mixture and let it mix thoroughly for approximately 2 s. Finally, we let the mixture stand for approximately 5 min to form AuNC/NMP nanohybrids. The resulting AuNC/NMP nanohybrid solution was centrifuged at 6,000 rpm for 30 min and washed with DI water at least three times to remove excess CTAC.

Preparation of hydrophilic AuNC/POE/NMP and hydrophobic AuNC/PIB-POE-POB/NMP nanohybrids

The first step was to prepare the amphiphilic polymer dispersant PIB-POE-PIB, which comprised Polyisobutylene-g-succinic anhydride (PIB-SA) with hydrophobic groups and poly(oxyethylene)-diamine (POE2000) with hydrophilic groups. Its preparation flowchart is shown in **Fig. S5, ESI**. These two materials were subjected to a ring-opening reaction of cyclic anhydrides in a tetrahydrofuran (THF) solution at a 2/1 mole ratio followed by a three-hour amidation reaction with the amine group (–NH₂) at 25 °C to form a mixture of organic

dispersants. Analysis was performed using Fourier transform infrared spectroscopy, as shown in **Fig. S6, ESI**. For the original anhydride functional group of PIB-SA, anhydride (C=O) stretching-vibration peaks appeared at 1710 cm⁻¹ and 1780 cm⁻¹. After the ring-opening reaction with POE2000, the anhydride stretching-vibration peaks disappeared, and the resulting amide functional group had a carbon–oxygen double bond at 1470 cm⁻¹ and –NH characteristic absorption peak at 1570 cm⁻¹. This was followed by a three-hour ring-closing reaction at 150 °C. At this time, the –NH stretching-vibration peak at 1570 cm⁻¹ disappeared, and the main absorption peaks of the imide functional group appeared at 1650 cm⁻¹ and 1710 cm⁻¹. The final product was concentrated under reduced pressure to remove THF, forming PIB-POE-PIB (dark brown solid). The changes in the molecular weights of the abovementioned materials were identified using gel permeation chromatography, as shown in **Fig. S7, ESI**. The number-average molecular weights (M_n) of PIB-SA and POE2000 were 1,369 and 2,301, respectively. For PIB-POE-PIB, M_n was 5,379, and the polydispersity index was 1.03. The results showed that PIB-SA was successfully grafted onto POE2000. Then, POE2000 and PIB-POE-PIB were mixed at different weight ratios into the NMPs. After continuous stirring for 30 min, POE/NMPs and PIB-POE-PIB/NMPs were obtained. Finally, we took equal amounts of POE/NMPs and PIB-POE-PIB/NMPs and stirred them with HAuCl₄ (0.01 M, 0.25 mL) in CTAC (0.1 M, 10 mL) for 1 h, added NaBr (0.01 M, 0.03 mL), and then slowly added the reducing agent, ascorbic acid (0.04 M, 0.09 mL), dropwise. Subsequently, we added the gold seed solution (0.065 mL) to the G1 solution (CTAC: 0.1 M, 10 mL; NaBr: 0.01 M, 0.01 mL; HAuCl₄: 0.01 M, 0.25 mL; ascorbic acid: 0.04 M, 0.09 mL) and stirred till the mixture turned light pink (approximately 10 s). We immediately added 0.3 mL of G1 to the mixture, mixed it thoroughly for 2 s, and let it stand for 5 min. The resulting AuNC/POE/NMP and AuNC/PIB-POE-POB/NMP nanohybrid solutions were centrifuged at 6,000 rpm for 30 min and washed repeatedly with DI water at least three times to remove excess CTAC. Finally, a hydrophilicity–hydrophobicity analysis was performed on the water contact angle of the final product for subsequent SERS detection.

Bacterial culture and SERS-substrate preparation

The bacterial species used in this study were *S. aureus*, which is a Gram-positive bacterium, and *E. coli*, which is a Gram-negative bacterium. Before culturing the bacteria, we used an autoclave to sterilize all glassware at high pressure and temperature (approximately 120 °C, 50 min). Broth and Lysogeny broth (LB) were prepared in a 250 mL serum bottle. We employed an inoculating loop to scoop out the *S. aureus* (ATCC 25923) strain into the broth (10 mL) and the *E. coli* strain into the LB (10 mL), and we incubated them at 37 °C for 18–24 h. Then, we pipetted 10 mL each of the broth and LB, poured them separately into sterilized test tubes for subculture, and placed them in a shaking incubator (120 rpm, 37 °C, 24 h). Finally, the optical density (OD) of the cultured bacteria was detected using UV-Vis light. The culture was diluted till OD₆₀₀ reached 0.6, and the growing bacterial colonies were counted. The bacterial solution was then centrifuged at 5,000 rpm for 3 min. The supernatant was removed and washed three times with phosphate-buffered saline

before it could be used for SERS detection. Next, AuNC, AuNC/NMP, AuNC/POE/NMP, and AuNC/PIB-POE-POB/NMP solutions (10 μ L) were drop-coated onto a clean 10 mm \times 10 mm aluminum sheet and heated in an oven to 80 $^{\circ}$ C. The analyte solution (10 μ L) was prepared by dissolving adenine at a concentration of 10^{-4} – 10^{-10} M. *S. aureus* (10 μ L) and *E. coli* (10 μ L) were mixed into a SERS substrate in a non-nutrient environment and dried for Raman detection.

Characterization and instruments

The XRD analyzer was tested using PSAXS-USH-WAXS-002. It used a Cu target with a characteristic wavelength (CuK α ray) of $\lambda=1.54056$ \AA and scanning diffraction angle 2θ ranging from 3° to 20° to observe the changes in the layers of clay. The UV-Vis spectra were tested using a spectrophotometer (UV-2450, Shimadzu, Kyoto, Japan). The synthesized nanohybrid solution was measured by the UV-Vis spectrometer to obtain the absorption peak of a specific wavelength to identify the reduction of AuNCs. The atomic force microscope (Dimension Icon, Bruker, USA) was used in tapping mode to scan and detect the thickness and phase images of Mica and delaminated clays (NMPs). The transmission electron microscope used in this study was JEM-2100 (JEOL, Tokyo, Japan). We dropped 10 μ L of the SERS substrate onto the copper grid, dried it at 80 $^{\circ}$ C for 24 h, and obtained transmission electron microscopy (TEM) images. Simulations were performed using finite-difference time-domain (Lumerical, Inc.) commercial software to obtain electromagnetic enhancement. High-resolution field-emission scanning electron microscopy (FE-SEM; JSM-6500Fa) was used. Test samples were prepared by dropping the samples on a clean glass surface and drying them in an oven at 80 $^{\circ}$ C for 2 h. Each sample was fixed with conductive carbon glue, and a thin layer of platinum was coated on the surface for FE-SEM photography. The confocal micro-Raman spectroscopy (LabRAM HR Evolution, Horiba, Kyoto, Japan) used a 633-nm-band laser with a measurement range of 400–2000 cm^{-1} . The exposure time was 10 s and the power was 20 mW. The excitation light was focused on an excitation area of approximately 4 μm using a 50 \times objective.

Results and Discussion

Synthesis and identification of gold nanocubes with different edge lengths

In this study, a seed-mediated method was improved and then used to prepare monodispersed AuNCs.⁴⁵²⁰ A schematic of the reduction process is shown in Fig. 1a. First, tetrachloroauric acid was reduced by sodium borohydride (NaBH_4) in the presence of CTAC to form a gold seed solution with a diameter of approximately 3–5 nm. Then, the growth solutions, namely G1 and G2, were prepared under the same CTAC conditions. CTAC acted as a protective agent to protect nanoparticles from aggregation during the reduction process. To induce anisotropic growth, increasing the growth rate along the (110) and (111) directions and simultaneously decreasing the growth rate along the (100) direction were necessary.¹⁸ Here, bromide has a fairly

strong affinity for the Au(100) facet.⁴⁶³⁴ Therefore, in the presence of CTAC, Br^- , which is advantageous for adsorption onto the (100) facet, was added, causing a difference in the growth rate between the (100) facet and other facets. When ascorbic acid was added, the solution turned colorless. Finally, the gold seed solution was added to G1. When G1 turned light pink (approximately 10 s), G1 had to be immediately transferred to G2 to stably generate AuNCs. This was followed by preliminary identification using a UV-Vis spectrometer, and its absorption spectra were collected every minute during the reduction process. As shown in Fig. 1b, AuNCs can be stably generated after approximately 5 min. G1 served as an important intermediate in the entire reduction process. In this study, we observed that the particle size of AuNCs can be effectively adjusted by changing the amount of G1 (0.1–0.5 mL). This is similar to the findings of previous literature: the size of particles grown by the seed-mediated method mainly depends on the number of seeds in the growth solution, and fewer gold seeds lead to a greater particle size. We chose to change the amount of G1 (the intermediate) because, as an enhanced seed solution, G1 turned red after a reaction time of approximately 20 s. At this time, the enhanced seed (G1) could not be used for further synthesis after its particle growth was completed.⁴⁷⁴² Therefore, based on cost considerations, we chose to change the amount of G1 solution added to avoid excessive consumption of intermediates. The absorption spectra of AuNCs with different edge lengths can be observed in Fig. 1c. As the edge length increased, its absorption wavelength gradually red-shifted. Therefore, adding different amounts of G1 solution enables the control of the size of AuNCs and the further adjust of the surface plasmon resonance (SPR) peaks. As shown in Fig. 1d, a linear regression was performed for the edge length and SPR peak, and R^2 reached 0.9947, indicating a good linear relationship between edge length and the SPR peak. Fig. 1e(1)–(5) shows the TEM images of AuNCs with different sizes. By measuring and calculating their average edge lengths via *Image J*, we observed that the size distribution of AuNCs was narrow, and their sizes exhibited a certain uniformity (Fig. 1e(6)–(10)). AuNCs with edge lengths from 33.90 nm to 65.26 nm can be obtained under the control of the added G1 amounts. The related UV-Vis absorption and average particle-size results are summarized in Table 1. The enhancement effect of SERS mainly depends on the LSPR of noble metals, which is in turn influenced by the morphology, size, and inter-particle distance of noble metallic nanoparticles. Therefore, we evaluated the effect of nanoparticle size on LSPR by adjusting the edge length of AuNCs. Adenine (biomolecule) was used for SERS analysis in this study. Fig. 1f shows the SERS detection of adenine at the same concentration (10^{-4} M) using AuNCs with different edge lengths at an excitation wavelength of 633 nm. The results suggest that the SERS-signal intensity was at its best when the average edge length was 38.34 nm, and the corresponding signal-to-background (S/B) ratio reached 2.0. The integrated intensities from the adenine characteristic peaks at 704–764 cm^{-1} are compared in Fig. S8, ESI. The SERS intensity was 2.14×10^5 for AuNCs with an average edge length of 38.34 nm. The results of the SERS intensity and S/B ratio are summarized in Table 1.

Among the size-distribution curves given by Fig. 1e(7), AuNCs with an average edge length of 38.34 nm had the narrowest distribution curve and the most uniform size distribution. The smaller the size of the AuNCs, the more AuNCs that can be irradiated by a laser in the same area. In this case, more hotspot areas were generated, thereby increasing the SERS-signal intensity. In the seed-mediated method, a larger number of enhanced gold seeds can produce smaller AuNCs. However, this also causes growth instability^{47,42} and more irregular shapes, thereby reducing the yield of AuNCs. Therefore, AuNCs with an

average edge length of 38.34 nm were used for subsequent applications. As shown in Fig. 1g, the limit of detection (LOD) of adenine by AuNCs was 10^{-8} M, demonstrating the extremely high sensitivity of AuNCs in SERS. In addition, the intensities at characteristic peaks of 704–764 cm^{-1} were integrated to quantify the LOD. The linear response between logarithmic integrated intensity and logarithmic concentration had a R^2 value of 0.9699 (Fig. 1h).

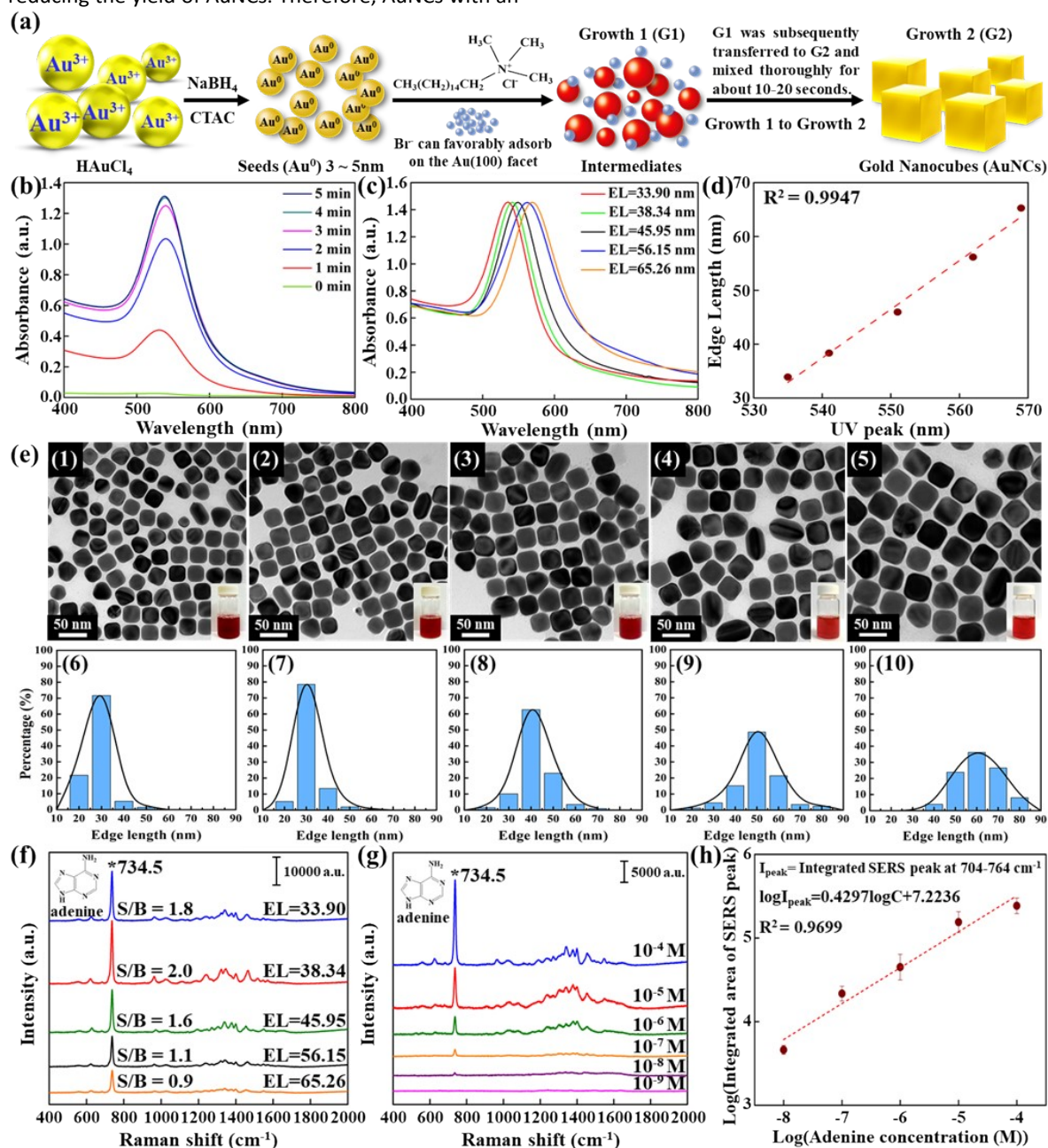


Fig. 1 (a) Schematic of the synthesis of gold nanocubes (AuNCs) using a seed-mediated method. First, a gold seed solution was synthesized in the presence of CTAC. Then, a two-step synthesis method was applied to perform quick reduction and stabilize the growth shape and size of AuNCs. (b) During the synthesis process, the UV-absorption spectra of AuNCs were obtained every minute. The entire reduction process only required 5 min to reach a stable state. (c) AuNCs with different edge lengths were synthesized by changing the content of the intermediate (G1) and were then detected using UV spectroscopy. (d) A linear regression was performed to obtain the correlation between the average edge length and UV-absorption peak of AuNCs, and R^2 reached 0.9947. (e) TEM images of AuNCs with different average edge lengths: (1) 33.90 nm, (2) 38.34 nm, (3) 45.95 nm, (4) 56.15 nm, and (5) 65.26 nm. In addition, (6)–(10) show the size-distribution diagrams of the AuNCs with different average edge lengths, which were measured and calculated using Image J. (f) SERS

spectra of same-concentration adenine (10^{-4} M) detected using AuNCs with various edge lengths. (g) LOD analysis of adenine detected using AuNCs with an average edge length of 38.34 nm. The LOD reached 10^{-8} M. (h) The intensities at characteristic peaks of $704\text{--}764\text{ cm}^{-1}$ were integrated to quantify the LOD, and a linear regression was performed between the logarithmic integrated intensity and logarithmic concentration. The R^2 value was 0.9699.

Table 1. Reduction of AuNCs with different edge lengths and their SERS intensity for adenine (biomolecule).

Sample	Zeta potential (mV)	UV-vis absorption (nm)	Average AuNC edge length (nm) ^a	SERS intensity ^b	S/B ratio ^c
AuNCs-1	+43.7	535	33.90	1.69×10^5	1.8
AuNCs-2	+44.8	541	38.84	2.14×10^5	2.0
AuNCs-3	+39.5	551	45.95	1.53×10^5	1.6
AuNCs-4	+41.9	562	56.15	9.57×10^4	1.1
AuNCs-5	+40.3	569	65.26	5.85×10^4	0.9

^a The average edge length of gold nanocubes were measured by TEM.

^b The integrated intensity range was $704\text{--}764\text{ cm}^{-1}$ and the concentration of adenine was 10^{-4} M.

^c The S/B ratio is defined as the amount of desired signal relative to the level of background signal in calculations using the equation $S/B\text{ ratio} = (\text{highest value} - \text{base value}) / \text{base value}$.

Preparation and identification of AuNCs/NMPs nanohybrids

The 2D nanomaterials are characterized by their uniform shape, high surface-area-to-volume ratio, and a large amount of charge on the surface. Among such nanomaterials, nanosilicate clay is often used as a chelating agent or stabilizer for metallic nanoparticles.⁴⁸⁵³⁻⁵⁰⁴⁷⁵ The clay we used in this study was Mica, of which a single flake is approximately $300\text{ nm} \times 300\text{ nm} \times 1\text{ nm}$. It has a large specific surface area and allows ion exchange. **Fig. 2a** shows the schematic of NMPs as a carrier for the stable growth of AuNCs. The gold particles were ion-exchanged under the surface charge of NMPs, and then the AuNCs were reduced onto the surface of NMPs through a seed-mediated method to form AuNCs/NMPs nanohybrids. **Fig. 2b** shows the absorption spectra during the reduction process, which was obtained using a UV-Vis light spectrometer. In the entire reduction process, AuNCs/NMPs were obtained in only approximately 6 min. This method can greatly reduce the time and cost of preparing AuNC nanohybrids. Next, the Zeta potential was used to detect the changes in surface potential values of AuNCs and AuNCs/NMPs before and after reduction, as shown in **Fig. 2c**. The original potential value of HAuCl_4 was +38.9 mV. The reduced AuNCs used the cationic surfactant CTAC as a solvent to protect the AuNCs from agglomeration, and the measured potential was +44.8 mV. Subsequently, the measured potential of the NMPs was -33.5 mV , and the final AuNC/NMP-nanohybrid product showed a potential of +41.3 mV. The changes in surface-potential values also indirectly proved that AuNCs were stably reduced on the NMP surface. To explore the stability and application of AuNCs in NMPs, we designed five different weight ratios, namely 5/1, 2/1, 1/1, 1/2, and 1/5. **Fig. 2d** shows the UV-Vis spectra at different weight ratios. When the content of NMPs increased, excess ionic charges affected the growth of the AuNCs. The UV spectra clearly show that the absorption-peak

intensity decreased, and the peak width tended to widen, indicating the inhomogeneity of the size and shape of the AuNCs. When the NMP content was too small, particles tended to agglomerate and stack. The TEM images in **Fig. 2e** also confirm that the reduction stability of anisotropic gold nanoparticles was poor when the NMP content was too large or too small. **Fig. 2e(2)** shows that AuNCs had good dispersion and alignment when the weight ratio was 2/1. In addition, EDS was used to identify the elemental composition of AuNCs/NMPs nanohybrids. As shown in **Fig. S9a, ESI**, the main element on their surface was Au, and elements such as Si, O, and Mg were all components of the NMPs. The EDS mapping in **Fig. S9b, ESI** also confirms that AuNCs were stable on the surface of the NMPs. Finally, the detection efficiencies of substrates at each weight ratio were obtained by detecting the adenine (biomolecule) at the same concentration (10^{-4} M). **Fig. 2f** shows the SERS spectra at various substrate weight ratios. The highest signal intensity was obtained at a weight ratio of 2/1, with an S/B ratio of 2.4. Moreover, the intensities at the adenine characteristic peaks of $704\text{--}764\text{ cm}^{-1}$ were integrated and compared. The SERS intensity exhibited by AuNCs/NMPs with a weight ratio of 2/1 reached 3.01×10^5 , as shown in **Fig. S10, ESI**. Therefore, the signal intensity of SERS was closely related to the number, arrangement, and spacing of noble metallic nanoparticles. The SERS-intensity results at each weight ratio are summarized in **Table 2**. Finally, the LOD in the case of the SERS substrate with the best detection effect is discussed. **Fig. 2g** shows that AuNCs/NMPs at a weight ratio of 2/1 presented an LOD of 10^{-9} M for adenine, and the intensities at characteristic peaks of $704\text{--}764\text{ cm}^{-1}$ were integrated to quantify the LOD. In the linear response between the logarithmic integrated intensity and logarithmic concentration (**Fig. 2h**), the R^2 value was 0.9840. After all the above steps were completed, the surface enhancement factor (EF) was used to calculate the sensitivity as follows:^{41386,34297}

$$EF = (I_{\text{SERS}} / C_{\text{SERS}}) / (I_{\text{norm}} / C_{\text{norm}}).$$

C_{norm} is the original adenine concentration in the focal-length range of the laser, which is 0.1 M; C_{SERS} is the limit concentration of adenine in the laser range on the SERS substrate; I_{norm} is the general Raman intensity; I_{SERS} is the SERS-signal intensity.

By integrating the intensities in the range of $704\text{--}764\text{ cm}^{-1}$, we obtained the optimal EF value, which was 3.6×10^8 . Based on the above results, we can observe that the AuNCs reduced on CTAC as a protective agent, and a good NMP carrier had a relatively regular arrangement, as shown in **Fig. 3a**. Additionally, the strong local electromagnetic-field effect generated at the tips of the AuNCs can effectively improve the sensitivity of the SERS signal.⁵¹⁴⁸⁶ The arrangement of particles can be clearly observed in the TEM images in **Fig. 3b**, which can effectively reduce the agglomeration phenomenon and the difficulty in controlling the spacing during the chemical reduction of metallic nanoparticles. We also randomly selected 50 points to detect the enhanced signal and calculate its RSD.

As shown in Fig. 3c, the RSD value was 10.7%, suggesting good reproducibility and stability of AuNCs/NMPs nanohybrids.

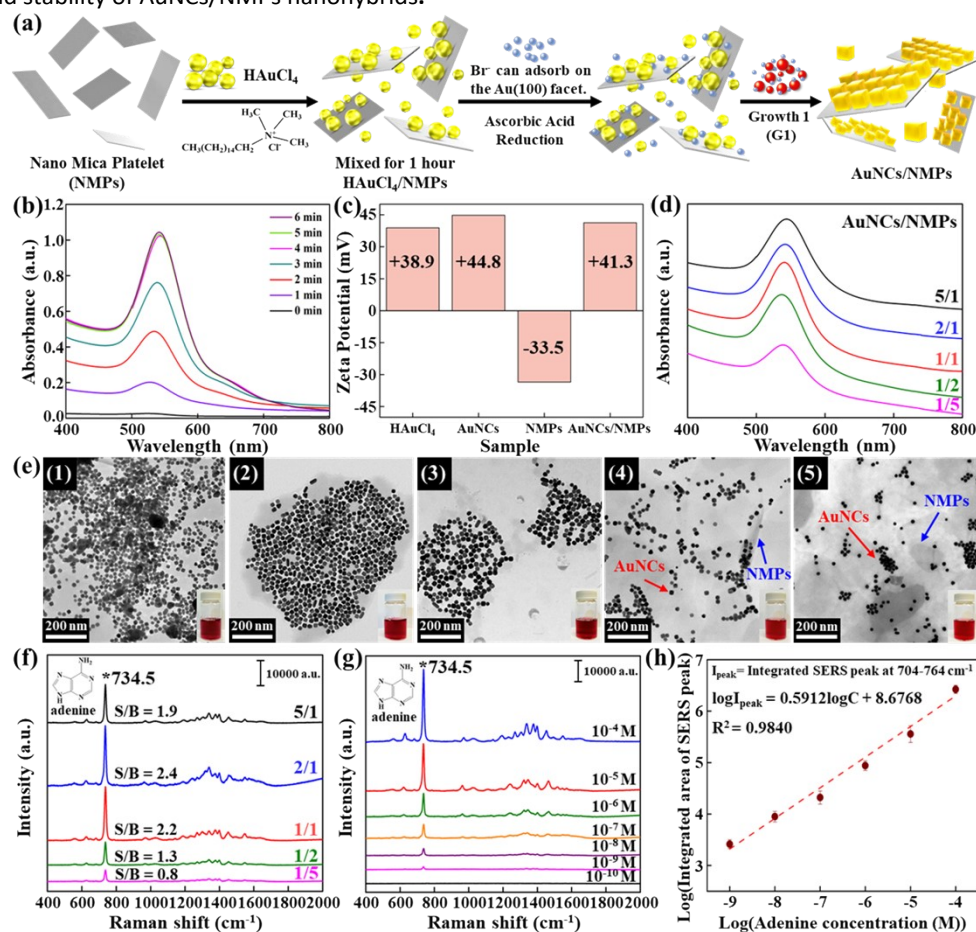


Fig. 2 (a) Schematic of the in-situ reduction of AuNCs on the surface of delaminated NMPs using a seed-mediated method. First, a cation-exchange reaction was carried out on the surface of Au^{3+} and NMPs to form an electrostatic attraction to stabilize the reduction and growth of AuNCs. Then, a two-step synthesis method was applied to quickly reduce and stabilize the growth shape and size of AuNCs. (b) The UV spectra of AuNCs/NMPs were collected every minute during the preparation process, where the weight ratio of AuNCs/NMPs was 1/1. (c) Zeta-potential spectra of HAuCl₄, AuNCs, NMPs, and AuNCs/NMPs. The changes in their surface potential values were detected, confirming that AuNCs grew stably on the surface of NMPs. (d) UV spectra of AuNC and NMP substrates synthesized at different weight ratios. (e) TEM images showing the distribution of AuNCs and NMPs at different weight ratios: (1) 5/1; (2) 2/1; (3) 1/1; (4) 1/2; and (5) 1/5. (f) SERS spectra of same-concentration adenine (10⁻⁴ M) detected using AuNCs/NMPs at each weight ratio. (g) LOD analysis when the weight ratio of AuNCs/NMPs was 2/1. The analytes were the SERS spectra of adenine at different concentrations. The LOD reached 10⁻⁹ M. (h) The intensities at characteristic peaks of 704–764 cm⁻¹ were integrated to quantify the LOD, and a linear regression was performed between logarithmic integrated intensity and logarithmic concentration. The R² value was 0.9840.

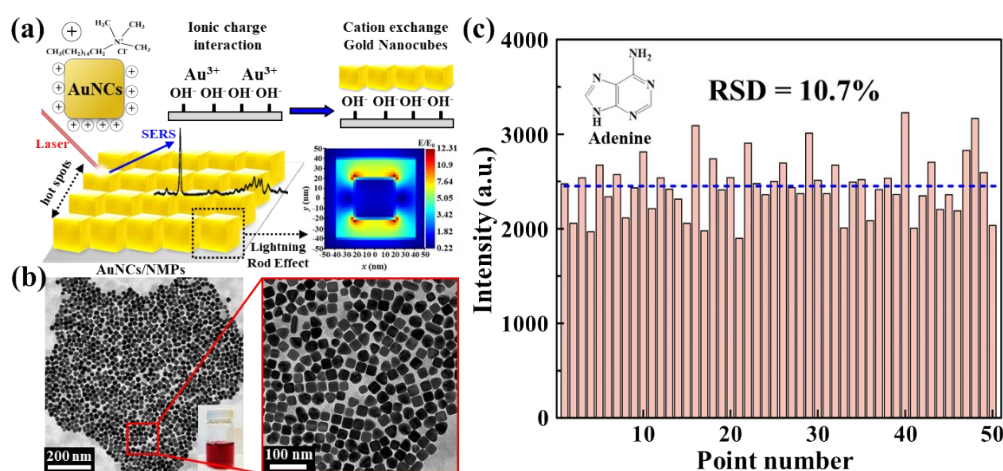


Fig. 3 (a) With CTAC as a protective agent and NMPs as a good carrier for stable nanoparticles, AuNCs were prepared using a chemical-reduction method, and the AuNCs were arranged with high regularity. The application of SERS enabled the production of an extremely high lightning-rod effect at the tips of AuNCs and greatly enhanced the signal intensity of SERS. (b) Furthermore, the TEM images show that the AuNCs/NMPs nanohybrids had good nanodispersion and a highly regular arrangement. (c) On the AuNCs/NMPs substrate with a weight ratio of 2/1, we randomly selected 50 points to detect the Raman signal and measure its intensity before calculating the RSD.

Table 2. Reduction of AuNCs/NMPs at different weight ratios and SERS intensity for adenine (biomolecule).

AuNCs/NMPs (weight ratio) ^a	Zeta potential (mV)	UV-vis absorption (nm)	Average AuNC edge length (nm) ^b	SERS intensity ^c	S/B ratio ^d
5/1	+47.5	544	-	1.85×10^5	1.9
2/1	+41.3	542	37.45	3.01×10^5	2.4
1/1	+38.6	540	38.66	2.49×10^5	2.2
1/2	+29.9	537	40.12	1.11×10^5	1.3
1/5	+20.1	539	-	5.68×10^4	0.8

^a The weight ratio was calculated on the basis of HAuCl₄/clay and weight ratios of 5/1, 2/1, 1/1, 1/2, and 1/5.

^b Average triangular nanoplate edge lengths of gold were measured by TEM.

^c The integrated intensity range was 704–764 cm⁻¹ and the concentration of adenine was 10⁻⁴ M.

^d The S/B ratio is defined as the amount of desired signal relative to the level of background signal in calculations using the equation S/B ratio = (highest value-base value)/base value.

Bacterial detection for SERS substrate with adjustable hydrophilicity and hydrophobicity

Fig. 4a conceptually shows the addition of POE2000 (hydrophilic polymer) onto the surface of delaminated NMPs to regulate the surface hydrophilicity and its application in the SERS detection of *S. aureus* (hydrophilic bacteria). Owing to the high ionic charge on the surface, NMPs adsorbed POE2000 through non-covalent ionic-charge interaction and van der Waals forces. Then, the surface hydrophilicity and hydrophobicity of the organic/inorganic nanohybrids were regulated by adding POE2000 with different weight ratios. Finally, the seed-mediated method was applied in the presence of POE/NMPs to generate AuNCs in situ, forming AuNCs/POE/NMPs nanohybrids. The absorption spectra of AuNCs/POE/NMPs nanohybrids at different weight ratios can be observed in **Fig. S11, ESI**. This figure simply proves that the reduction of AuNCs was stable with the addition of POE2000. **Fig. 4b** shows the hydrophilicity analysis for the water contact angle under different POE2000 contents. Without the addition of POE2000, the water contact angle of AuNCs/NMPs was 37.5° because the polar structure of the clay-silica bond made the surface of the NMPs hydrophilic. As the content of POE2000 increased, the contact angle decreased from 37.5° to 14.0°, indicating that nanohybrids tended to become increasingly hydrophilic. In addition, we tested the contact angle of diiodomethane on the surfaces of AuNCs/POE/NMPs and calculated the surface free energy of AuNCs/POE/NMPs using the Owens–Wendt surface energy:⁵²⁴⁹⁷

$$\gamma_L(1 + \cos\theta) = 2\sqrt{\gamma_S^d \gamma_L^d} + 2\sqrt{\gamma_S^p \gamma_L^p}$$

where γ_S and γ_L denote the surface free energy of solids and pure liquids, respectively, and the superscripts d and p represent the contributions of dispersion and non-dispersion to

the total surface energy, respectively. The following parameters were used in this study: water ($\gamma_L^d = 72.8$ mJ/m², $\gamma_L^p = 21.8$ mJ/m², $\gamma_L^d = 51$ mJ/m²) and diiodomethane ($\gamma_L^d = 50.8$ mJ/m², $\gamma_L^p = 48.5$ mJ/m², $\gamma_L^d = 2.3$ mJ/m²). Finally, we calculated the surface free energy of AuNCs/POE/NMPs as follows:⁵²⁴⁹⁷

$$\gamma_S = \gamma_S^d + \gamma_S^p$$

The calculation results are listed in **Table 3**. The results show that as the content of POE2000 increased, the surface free energy γ_S of the AuNCs/POE/NMPs increased from 59.47 mJ/m² to 72.80 mJ/m². Then, we performed a SERS spectral analysis of AuNCs, AuNCs/NMPs, and AuNCs/POE/NMPs at various weight ratios for *S. aureus* (ATCC 25923), as shown in **Fig. 4c**. The test results show that the best SERS-signal results were obtained in the case of adding NMPs compared with not adding NMPs. This was mainly because the surface hydrophilicity enabled the NMPs to adsorb *S. aureus* well with similar polar molecules. When the weight ratio was 2/1/1, the SERS intensity for *S. aureus* (characteristic peak at 733 cm⁻¹) reached 2.63×10^4 , as shown in **Fig. S12, ESI**. Typically, the SERS spectra of Gram-positive bacteria exhibit prominent peaks at 733, 1330, and 1460 cm⁻¹, while the peaks at 660, ~73025, 1095, 1330, and 1460 cm⁻¹ stand out in those of Gram-negative ones. Specifically, the most conspicuous peak at 733 cm⁻¹ in the SERS spectra of Gram-positive *S. aureus* and the corresponding doublet at 660 and ~73025 cm⁻¹ in that of Gram-negative *E. coli* were exploited as their respective biomarkers in SERS-based susceptibility testing.⁵³⁻⁵⁵ The surface free energy γ_S of *S. aureus* (ATCC 25923) at pH 7 was 60.05 mJ/m²,⁵⁶³⁰⁴⁸ which was similar to that of AuNCs/POE/NMPs (60.95 mJ/m² at 2/1/1). This shows that the SERS-signal intensity for detecting *S. aureus* depended on the surfactant content in AuNC/POE/NMP nanohybrids. Finally, the concentration of *S. aureus* was diluted to 9.2×10^7 CFU/mL, followed by the SERS detection of the LOD (**Fig. 4d**). The results showed that the LOD of AuNPs/POE/NMPs with a weight ratio of 2/1/1 for *S. aureus* reached 92 CFU/mL. In the linear response between logarithmic intensity and logarithmic concentration in **Fig. 4e**, the R² value was 0.9925. This result also suggested that SERS provided sufficient sensitivity in terms of the LOD and linear range of detection, and it exhibited excellent performance in sensitivity and detection time.

Fig. 5a shows the addition of amphiphilic polymer PIB–POE–PIB to the surface of delaminated NMPs to regulate the surface hydrophilicity and its application in the SERS detection of *E. coli* (hydrophobic bacteria). NMPs comprise silicon–oxygen bonds, which are characterized by a polar structure. Owing to this structure, the clay surface is hydrophilic and has poor compatibility and interaction with hydrophobic molecules. Therefore, the amphipathic polymer PIB–POE–PIB was used to modify the surface of NMPs via non-covalent ionic charge interactions and van der Waals forces. Finally, AuNCs were also generated in situ via seed-mediated reduction in the presence of PIB–POE–PIB/NMPs, thereby forming AuNCs/PIB–POE–PIB/NMPs nanohybrids. The absorption spectra of AuNCs/PIB–

POE-PIB/NMPs nanohybrids at different weight ratios can be observed in **Fig. S13, ESI**. The figure shows that the reduction situation of AuNCs was stable for different amounts of added PIB-POE-PIB. However, too much PIB-POE-PIB would lead to an NMP solution that is too viscous and unable to stably generate AuNCs. Therefore, we did not prepare a nanohybrid at a 2/15/1 ratio. **Fig. 5b** shows the hydrophobicity analysis of the water contact angle under different PIB-POE-PIB contents. The original AuNCs/NMPs exhibited a water contact angle of 37.5°. As the content of PIB-POE-PIB increased, the contact angle increased from 37.5° to 60.1°, indicating that the nanohybrids became more hydrophobic. In addition, the contact angle of diiodomethane on the surface of AuNCs/PIB-POE-PIB/NMPs was also tested, and the surface free energy of AuNCs/PIB-POE-PIB/NMPs was calculated using the Owens-Wendt surface energy. The results are presented in **Table 4**. We can observe from **Table 4** that as the content of PIB-POE-PIB increased, the surface free energy γ_s of the AuNCs/PIB-POE-PIB/NMPs decreased from 59.47 mJ/m² to 40.97 mJ/m². Next, a SERS spectral analysis of *E. coli* (ATCC 25922) was performed at various weight ratios of AuNCs, AuNCs/NMPs, and AuNCs/PIB-

POE-PIB/NMPs. **Fig. 5c** shows that for AuNCs or the addition of NMPs, the SERS-signal intensities of *E. coli* were considerably weak. The hydrophilic nature of NMP surfaces led to a poor adsorption capacity for hydrophobic *E. coli*. Therefore, by changing the hydrophilic-hydrophobic properties of the clay surface, the SERS intensity for *E. coli* (at a characteristic peak of 730 cm⁻¹) reached 6.01×10^3 when the weight ratio was 2/10/1 (**Fig. S14, ESI**). The surface of *E. coli* (ATCC 25922) was hydrophobic, and the surface free energy γ_s at pH 7 was 39.70 mJ/m²,⁵⁷⁴¹⁴⁹ which was most similar to that of the AuNCs/PIB-POE-PIB/NMPs (40.97 mJ/m²) at 2/10/1. Finally, the concentration of *E. coli* was diluted to 1.6×10^8 CFU/mL, and the limit concentration was detected by SERS (**Fig. 5d**). The results showed that the LOD of AuNCs/PIB-POE-PIB/NMPs with a weight ratio of 2/10/1 reached 1.6×10^2 CFU/mL. In the linear response between logarithmic intensity and logarithmic concentration in **Fig. 5e**, the R² value was 0.9844. Moreover, the addition of the amphiphilic polymer PIB-POE-PIB made the surfaces of the nanohybrids more hydrophobic; thus, they had a higher affinity for contact with the surfaces of hydrophobic bacteria. This was reflected in the SERS enhancement effect.

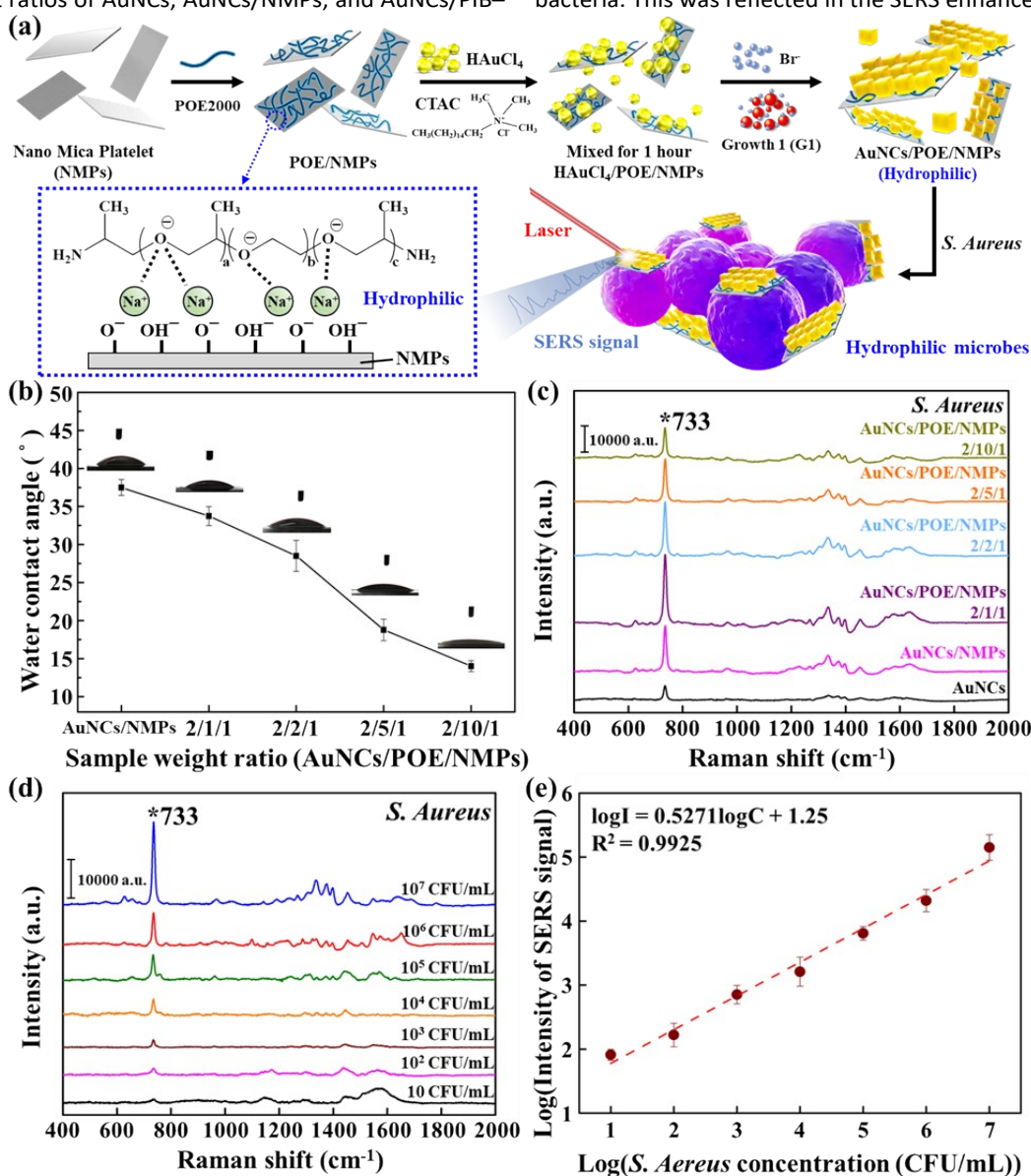


Fig. 4 (a) Schematic of regulating hydrophilic AuNC/POE/NMP nanohybrids for the SERS detection of *S. aureus* (hydrophilic bacteria). First, POE2000 was mixed on the surface of the NMPs through non-covalent interaction. Then, AuNCs were generated via in-situ reduction, and their growth was stabilized. Finally, they were applied to the SERS detection of *S. aureus* (hydrophilic bacteria). (b) Plot of the water contact angle of AuNCs/POE/NMPs with different weight ratios. (c) SERS spectra of *S. aureus* at various weight ratios of AuNCs, AuNCs/NMPs, and AuNCs/POE/NMPs. Among them, AuNCs/POE/NMPs with a weight ratio of 2/1/1 yielded the best detection effect. (d) SERS spectra for the LOD analysis of *S. aureus* at different concentrations. (e) The logarithmic concentration and signal intensity of the analyte were plotted to observe their linear relationship.

Table 3. Contact angle and surface free energy of AuNCs/NMPs and AuNCs/POE/NMPs with different added amounts of the hydrophilic surfactant POE2000.

Sample name	Contact angle (°)		Surface free energy (mJ/m ²)		
	Water	CH ₂ Cl ₂	γ_S^d	γ_S^p	γ_S
AuNCs/NMPs	37.5	43.8	25.01	36.46	59.47
AuNCs/POE/NMPs 2/1/1	35.7	40.4	26.48	34.47	60.95
AuNCs/POE/NMPs 2/2/1	28.5	14.6	35.23	32.43	67.66
AuNCs/POE/NMPs 2/5/1	18.8	14.2	34.29	37.13	71.42
AuNCs/POE/NMPs 2/10/1	14.0	13.9	33.97	38.83	72.80

Note: The surface free energy γ_S of *S. aureus* (ATCC 25923) at pH 7 was 60.05 mJ/m².⁵⁶³⁰⁴⁸

Table 4. Contact angle and surface free energy of AuNCs/NMPs and AuNCs/PIB-POE-PIB-NMPs with different amounts of the amphipathic surfactant PIB-POE-PIB.

Sample name	Contact angle (°)		Surface free energy (mJ/m ²)		
	Water	CH ₂ Cl ₂	γ_S^d	γ_S^p	γ_S
AuNCs/NMPs	37.5	43.8	25.01	36.46	59.47
AuNCs/PIB-POE-PIB/NMPs 2/1/1	39.3	41.6	26.36	32.32	58.68
AuNCs/PIB-POE-PIB/NMPs 2/2/1	43.3	43.7	25.95	29.98	55.93
AuNCs/PIB-POE-PIB/NMPs 2/5/1	51.7	50.4	23.67	25.75	49.42
AuNCs/PIB-POE-PIB/NMPs 2/10/1	60.1	70.1	14.15	26.82	40.97

Note: The surface free energy γ_S of *E. coli* (ATCC 25922) at pH 7 was 39.70 mJ/m².⁵⁷⁴⁴⁴⁹

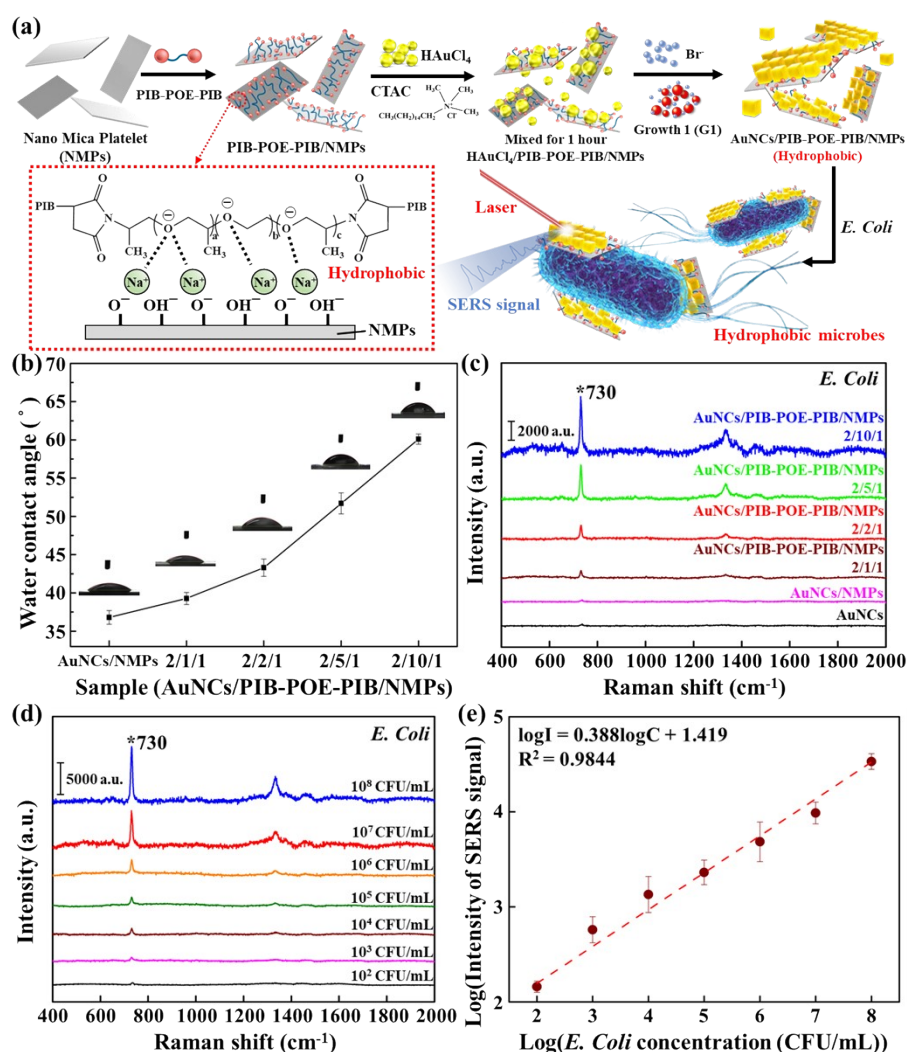


Fig. 5 (a) Schematic of regulating hydrophobic AuNCs/PIB-POE-PIB/NMPs nanohybrids for SERS detection of *E. coli* (hydrophobic bacteria). First, PIB-POE-PIB was mixed on the surface of the NMPs through non-covalent interaction. Then, AuNCs were generated via in-situ reduction, and their growth was stabilized. Finally, they were applied to the SERS detection of *E. coli* (hydrophobic bacteria). (b) Plot of the water contact angle of AuNCs/PIB-POE-PIB/NMPs with different weight ratios. (c) SERS spectra of *E. coli* detected by AuNCs, AuNCs/NMPs, and AuNCs/PIB-POE-PIB/NMPs at various weight ratios. Among them, AuNCs/PIB-POE-PIB/NMPs with a weight ratio of 2/10/1 yielded the best detection results. (d) SERS spectra of *E. coli* subjected to LOD analysis at different concentrations. (e) The logarithmic concentration and signal intensity of the analyte were plotted to observe their linear relationship.

Adsorption capacity of bacteria on hydrophilic–hydrophobic SERS substrates

S. aureus is a Gram-positive bacterium, and the teichoic acid in its cell wall makes its bacterial surface hydrophilic. *E. coli* is a Gram-negative bacterium, and its cell wall does not contain teichoic acid; however, the hydrophobic surface of its outer membrane comprising LPS and protein makes the surface of *E. coli* hydrophobic. The cell-wall structures of both *S. aureus* and *E. coli* make their surfaces negatively charged. The Zeta potentials of the *S. aureus* and *E. coli* surfaces are -33.2 mV and -45.9 mV, respectively. *E. coli* has a higher negative surface-charge value due to the presence of an LPS layer on its surface.^{58520–615853} According to the previously mentioned synthesis process of SERS substrates, CTAC is used as a protective agent to coat the AuNCs, making the substrates' surface positively charged. CTAC is used as a protective agent to coat the AuNCs, which makes the surface of the substrates positively charged. Therefore, AuNCs have a better adsorption effect on negatively charged molecules on the surface. As briefly described in **Fig. 6a**, bacteria with different hydrophilic–hydrophobic properties can be physically adsorbed by controlling the hydrophilicity and hydrophobicity of nanohybrid surfaces and utilizing the principle of positive- and negative-charge adsorption. In this study, we used two types of polymers, namely hydrophilic polymer poly(oxyethylene)-diamine (POE2000)^{62596,63057} and amphiphilic polymer PIB–POE–PIB. The structure of PIB–POE–PIB is a triblock polymer with hydrophobic groups at both ends and a hydrophilic group in the middle. The hydrophilic groups can adsorb to the surface of NMPs, while the hydrophobic groups at both ends can change the hydrophilic–hydrophobic characteristics of the surface. Therefore, bacteria are captured through physical adsorption for subsequent SERS detection. **Fig. 6b**, **Fig. 6c**, and **Video S1**, **ESI** show the physical capture of *S. aureus* and *E. coli* on each substrate, respectively. After 24 h of culture, we added the bacteria to each SERS substrate and let them stand for 30 min. The results showed that the test tube without the substrate was still turbid (the leftmost in the figure), and each substrate had adsorbed bacteria and gradually precipitated. The precipitation effect was most obvious when the weight ratio of AuNCs/POE/NMPs was 2/1/1 (**Fig. 6b**). In addition, NMPs are hydrophilic in nature; thus, they did not have a good adsorption capacity for hydrophobic bacteria. We can also clearly observe from **Fig. 6c** that compared with other turbid test tubes, the AuNCs/PIB–POE–PIB/NMPs at a weight ratio of 2/10/1 had the best capture ability, and its supernatant confirmed that bacteria were adsorbed to the bottom. The adsorption of bacteria to the SERS substrate was observed using FE-SEM. The surface of the original *S. aureus* (with no substrate added) was smooth, as shown in **Fig. 6d(1)**. **Fig. 6d(2)–(4)** shows the SEM images of *S. aureus* coated by AuNCs/POE/NMPs with a weight ratio of 2/1/1 at different contact times. The surrounding area of *S. aureus* was clearly coated by AuNCs/POE/NMPs (white protrusions), and the coated area increased with the time of contact. **Fig. 6e(1)** shows the original *E. coli* with no substrate coated. **Fig. 6e(2)–(4)** shows SEM images of *E. coli* coated by AuNCs/PIB–POE–PIB/NMPs with a weight ratio of 2/10/1 at different contact times; these figures also show that the coated area became larger with longer contact times. The results confirmed that bacteria can be easily captured through physical adsorption and used for SERS spectral analysis. Due to the abundant ionic charges on the surface of NMPs, these nanohybrid substrates exhibit the capability to inhibit bacterial growth without compromising the surface structure of bacteria and the structure of the detected substances.^{62596,63057} Therefore, while bacterial viability is affected, the SERS detection effectiveness remains unaffected at a

constant concentration. **Fig. S15** and **Fig. S16**, **ESI** illustrate bacterial detection using SERS substrates with different hydrophilicity and hydrophobicity, respectively. **Fig. S17**, **ESI** is the SERS spectra using the PCA algorithm. Loading profiles of LD1–LD2 indicated the potential for distinguishing *S. aureus* and *E. coli*. The detection results all confirmed the high sensitivity and high selectivity of the substrates. Finally, we also sorted and compared the recently reported detection of DNA molecules adenine and bacteria using gold nanoparticles and hybrids comprising different types of gold particles, as shown in **Table S1**, **ESI**. As presented in **Table S1**, relatively few studies have been conducted on polymorphic gold on adenine (biomolecule). Most existing studies add organic or inorganic materials to form a SERS substrate composed of hybrid materials, and its LOD can reach 10^{-9} M. In this study, the detection effect of adenine was excellent in terms of both the LOD and EF value. In addition, many studies focusing on bacterial detection added antibodies or aptamers to increase the capture of bacteria. Although the overall SERS detection limit has been greatly improved, the price of antibodies is relatively high due to economic and cost considerations. AuNCs/POE/NMPs and AuNCs/PIB–POE–PIB/NMPs nanohybrids can adsorb bacteria through physical capture, and their cost is relatively low. Therefore, they have great application value for SERS bacterial detection.

Conclusions

This study successfully prepared AuNCs through a seed-mediated method and reduced them on the surface of 2D delaminated NMPs to form AuNCs/NMPs nanohybrids with a 3D lightning-rod effect. By changing the amount of growth solution added, we could ensure an average particle size of AuNCs ranging between 30 nm and 70 nm. The surface of NMPs was rich in ionic charges and provided a large specific surface area to stabilize the growth of AuNCs. The delaminated AuNCs/NMPs nanohybrids generated 3D hotspot effects through self-assembly to enhance Raman signals. The detection of adenine (biomolecule) through SERS was highly sensitive. Its LOD reached 10^{-9} M, the Raman EF value was 3.6×10^8 , and RSD was 10.7%. This approach addresses previous drawbacks such as the prolonged synthesis time and overly complicated steps involved in the preparation of AuNCs. Simultaneously, by capitalizing on the physical capturing effect, it enhances the contact between analytes and noble metal nanoparticles, significantly amplifying the overall SERS signal. In this study, considering material properties and cost reduction, we designed an organic/inorganic nano-dispersed hybrid SERS substrate, conducting further spectral analysis on bacterial strains with different hydrophilic-hydrophobic characteristics. Finally, the hydrophilic polymer POE2000 and amphiphilic polymer PIB–POE–PIB were added in different weight ratios to modify the surface of the NMPs. The surface hydrophilicity and hydrophobicity of the AuNC/NMP nanohybrids were adjusted to achieve good adsorption and selectivity for bacteria. The AuNCs/POE/NMPs and AuNCs/PIB–POE–PIB/NMPs were further applied to the SERS detection of hydrophilic *S. aureus* and hydrophobic *E. coli*, respectively. The SERS-detection performance was good; the LOD of *S. aureus* reached 92 CFU/mL, and that of *E. coli* reached 1.6×10^2 CFU/mL. These results confirmed that AuNCs/POE/NMPs and AuNCs/PIB–POE–PIB/NMPs nanohybrids can significantly improve the detection selectivity and sensitivity for bacteria with different hydrophilic–hydrophobic properties. Therefore, the

AuNCs/NMPs nanohybrids in this study provide fast, highly selective, and highly sensitive detection results in the field of SERS biodetection.

Conflicts of interest

There are no conflicts to declare.

Acknowledgements

This research was funded by the National Science and Technology Council (MOST 111-2628-E-011-009-MY3, NSTC 112-2221-E-011-004-MY3, and NSTC 113-2622-8-011-007-TE2) of Taiwan.

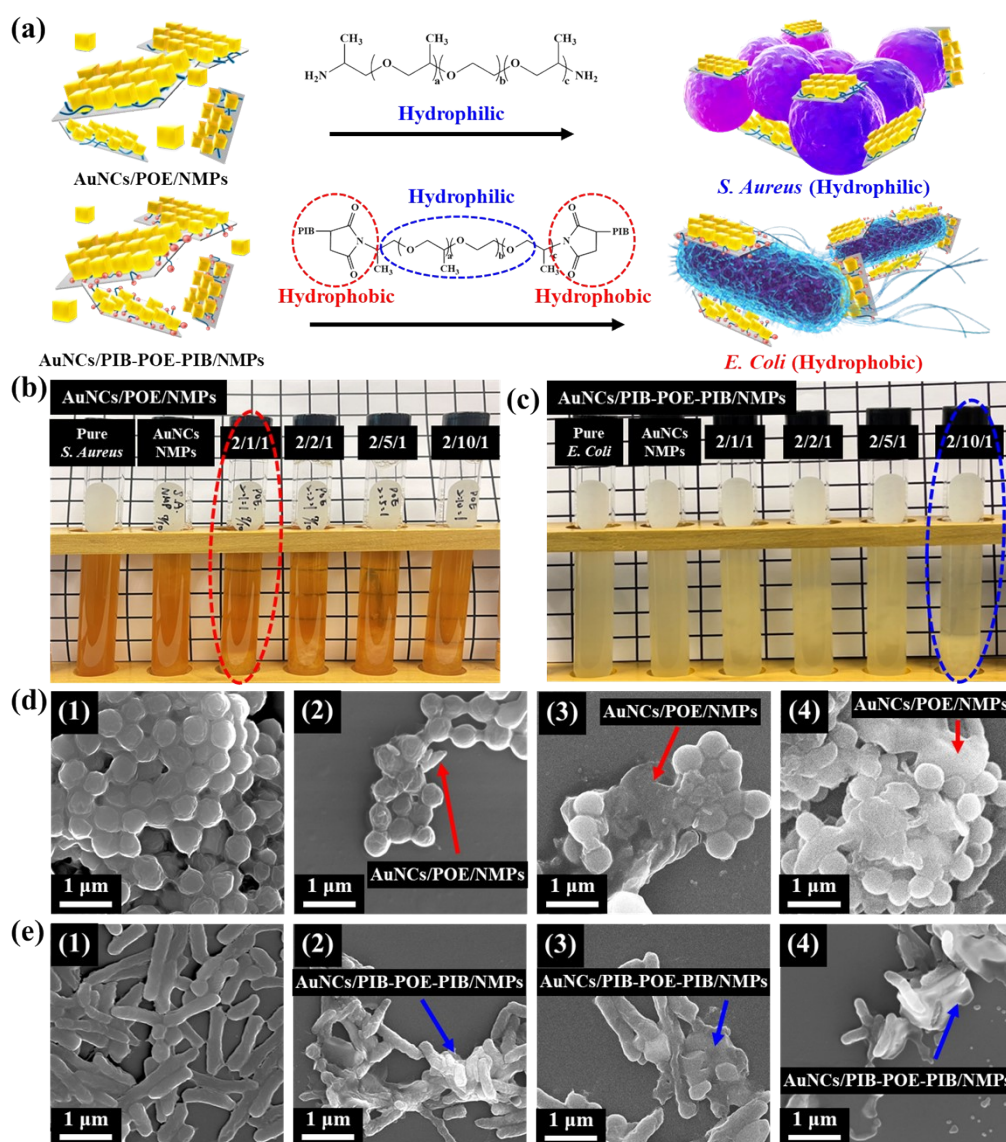


Fig. 6 (a) Schematic of the NMPs being adsorbed onto the surface of *S. aureus* and *E. coli* after their surface hydrophilicity and hydrophobicity were modified. When the hydrophilic polymer POE2000 was added to increase the hydrophilicity of the surface of NMPs, NMPs could adsorb hydrophilic *S. aureus* well. In addition, the amphiphilic polymer PIB-POE-PIB is a triblock polymer with hydrophobic groups at both ends and a hydrophilic group in the middle. The surface of NMPs can be modified to be relatively hydrophobic; thus, it can also adsorb hydrophobic *E. coli* well. (b) Each substrate physically captured *S. aureus*. After addition, AuNCs/POE/NMPs with a weight ratio of 2/1/1 yielded the best adsorption effect. (c) Each substrate physically captured *E. coli*. After addition, AuNCs/PIB-POE-PIB/NMPs with a weight ratio of 2/10/1 obtained the best adsorption effect. (d) SEM images of *S. aureus* when AuNCs/POE/NMPs with a weight ratio of 2/1/1 were added. (e) SEM images of *E. coli* when AuNCs/PIB-POE-PIB/NMPs with a weight ratio of 2/10/1 were added. Image (1) shows pure bacteria without adding any substrate. After a culture of 24 h, the bacteria were added to the SERS substrates and left to stand for (2) 30 min, (3) 60 min, and (4) 90 min.

Notes and references

- 1 A. Amirjani, P. Shokrani, S. A. Sharif, H. Moheb, H. Ahmadi, Z. S. Ahmadiani, and M. S. Paroushi, *J. Mater. Chem. B*, 2023, **11**, 3537–3566.
- 2 G. Demirel, H. Usta, M. Yilmaz, M. Celik, H. A. Alidagi and F. Buyukserin, *J. Mater. Chem. C*, 2018, **6**, 5314–5335.
- 3 P. Verma, R. K. Wanchoo and A. P. Toor, *Chem. Eng. J.*, 2022, **430**, 132550.
- 4 A. R. Deshmukh, H. Aloui and B. S. Kim, *Chem. Eng. J.*, 2021, **421**, 127859.
- 5 W. Wang, J. Wang and Y. Ding, *J. Mater. Chem. B*, 2020, **8**, 4813–4830.
- 6 S. Yadav and J. Satija, *J. Mater. Chem. B*, 2021, **9**, 267–282.
- 7 L. Zeng, X. Xu, H. Ding, S. Song, L. Xu, C. Xu and H. Kuang, *J. Mater. Chem. B*, 2022, **10**, 909–914.
- 8 L. Zhang, Y. Mazouzi, M. Salmain, B. Liedberg and S. Boujday, *Biosens. Bioelectron.*, 2020, **165**, 112370.
- 9 M. Q. He, Y. L. Yu and J. H. Wang, *Nano Today*, 2020, **35**, 101005.
- 10 L. Liu, A. Thakur, W. K. Li, G. Qiu, T. Yang, B. He, Y. Lee and C. M. L. Wu, *Chem. Eng. J.*, 2022, **446**, 137383.
- 11 Z. Fusco, M. Rahmani, R. Bo, T. Tran-Phu, M. Lockrey, N. Motta, D. Neshev and A. Tricoli, *Adv. Funct. Mater.* 2019, **29**, 1806387.
- 12 J. H. Kim, S. Cha, Y. Kim, J. Son, J. E. Park, J. W. Oh and J. M. Nam, *Nano Lett.*, 2021, **21**, 7512–7518.
- 13 M. Yu, Q. Tian, G. He, K. Cui and J. Zhang, *Adv. Fiber Mater.*, 2021, **3**, 349–358.
- 14 P. Malik, D. Sarker, D. Kumar, M. Schwartzkopf, P. Srivastava and S. Ghosh, *ACS Appl. Mater. Interfaces*, 2023, **15**, 45426–45440.
- 15 E. Oksenberg, I. Shlesinger, G. Tek, A. F. Koenderink and E. C. Garnett, *Adv. Mater.*, 2023, **33**, 2211154.
- 16 Y. K. Xu, S. Hwang, S. Kim and J. Y. Chen, *ACS Appl. Mater. Interfaces*, 2014, **6**, 5619–5628.
- 17 A. Umar, J. Kim and S. M. Choi, *Cryst. Growth Des.*, 2021, **21**, 4133–4140.
- 18 J. E. Park, Y. Lee and J. M. Nam, *Nano Lett.*, 2018, **18**, 6475–6482.
- 19 C. W. Chiu, T. K. Huang, Y. C. Wang, B. G. Alamani and J. J. Lin, *Prog. Polym. Sci.*, 2014, **39**, 443–485.
- 20 X. Chen, and J. H. Ahn, *J. Mater. Chem. B*, 2020, **8**, 1082–1092.
- 21 D. Chimene, D. L. Alge and A. K. Gaharwar, *Adv. Mater.*, 2015, **27**, 7261–7284.
- 22 Y. F. Chen, C. H. Wang, W. R. Chang, J. W. Li, M. F. Hsu, Y. S. Sun, T. Y. Liu, and C. W. Chiu, *ACS Appl. Bio Mater.*, 2022, **5**, 1073–1083.
- 23 C. W. Chiu and P. H. Lin, *RSC Adv.*, 2015, **5**, 86522–86528.
- 24 C. W. Chiu and Lin, P. H. *RSC Adv.*, 2016, **6**, 67204–67211.
- 25 Y. C. Lee and C. W. Chiu, *Nanomaterials*, 2019, **9**, 324.
- 26 C. Yu, P. Zhang, J. Wang and L. Jiang, *Adv. Mater.*, 2017, **29**, 1703053.
- 27 C. Cheng, W. Bai, T. Zhu, W. Zang, S. Chen, J. Sun and D. Wang, *J. Mater. Chem. B*, 2021, **9**, 1804–1810.
- 28 H. Hu, J. Wang, X. Yi, K. Lin, S. Meng, X. Zhang, C. Jiang, Y. Tang, M. Wang, J. He, X. YU and Y. Song, *Anal. Methods*, 2022, **14**, 4014–4020.
- 29 Y. Liu, X. Wang, X. Fan, M. Ge, L. Fang, Y. Yuan, L. Chen, J. Jiang, A. Cao and L. Gao, *Adv. Funct. Mater.*, 2023, **33**, 2212655.
- 30 X. Zhang, P. Wu, X. Hao, J. Liu, Z. Huang, S. Weng, W. Chen, L. Huang and J. Huang, *J. Mater. Chem. B*, 2023, **11**, 7696–7706.
- 31 Y. Huang, Y. Chen, Z. Lu, B. Yu, L. Zou, X. Song, H. Han, Q. Jin and J. Ji, *Small*, 2023, **19**, 2302578.
- 32 J. Vergalli, I. V. Bodrenko, M. Masi, L. Moynié, S. Acosta-Gutierrez, J. H. Naismith, A. Davin-Regli, M. Ceccarelli, B. van den Berg, M. Winterhalter and J. M. Pagès, *Nat. Rev. Microbiol.*, 2020, **18**, 164–176.
- 33 H. Zhou, D. Yang, N. E. Mircescu, N. P. Ivleva, K. Schwarzmeier, A. Wieser, S. Schubert, R. Niessner and C. Haisch, *Microchim. Acta*, 2015, **182**, 2259–2266.
- 34 N. E. Dina, H. Zhou, A. Colniță, N. Leopold, T. Szoke-Nagy, C. Coman and C. Haisch, *Analyst*, 2017, **142**, 1782–1789.
- 35 M. A. Tahir, X. Zhang, H. Cheng, D. Xu, Y. Feng, G. Sui, H. Fu, V. K. Valev, L. Zhang and J. Chen, *Analyst*, 2020, **145**, 277–285.
- 36 N. E. Mircescu, H. Zhou, N. Leopold, V. Chiș, N. P. Ivleva, R. Niessner, A. Wieser and C. Haisch, *Anal. Bioanal. Chem.*, 2014, **406**, 3051–3058. R. Jones, C. Mijsch, H. Kwon, C. Pothoven, K. R. Rusimova, M. Kamp, K. Gong, L. Zhang, T. Batten, B. Smith, A. V. Silhanek, P. Fischer, D. Wolverson and V. K. Valev, *Adv. Mater.*, 2023, **35**, 2370244.
- 37 D. Yang, H. Zhou, N. E. Dina and C. Haisch, *Royal Soc. Open Sci.*, 2018, **5**, 1809555. Liu, Q. Hu, C. Li, F. Zhang, H. Gu, X. Wang, S. Li, L. Xue, T. Madl, Y. Zhang and L. Zhou, *ACS Sens.*, 2021, **6**, 2911–2919.
- 38 K. Yuan, J. Zheng, D. Yang, B. Jurado Sanchez, X. Liu, X. Guo, C. Liu, N. E. Dina, J. Jian, Z. Bao, Z. Hu, Z. Liang, H. Zhou and Z. Jiang, *ACS omega*, 2018, **3**, 2855–2864.
- 39 M. A. Tahir, N. E. Dina, H. Cheng, V. K. Valev and L. Zhang, *Nanoscale*, 2021, **13**, 11593–11634.
- 40 C. W. Chiu, Y. C. Lee, G. B. Ou and C. C. Cheng, *Ind. Eng. Chem. Res.*, 2017, **56**, 2935–2942.
- 41 W. R. Chang, C. Hsiao, Y. F. Chen, C. F. J. Kuo and C. W. Chiu, *ACS Omega*, 2022, **7**, 41815–41826.
- 42 Y. F. Chen, W. R. Chang, J. H. Wang, C. F. J. Kuo, C. C. Cheng and C. W. Chiu, *ACS Appl. Nano Mater.*, 2023, **6**, 13604–13615.
- 43 Z. Zhuang, Z. Li, G. Gong, Q. Li, Y. Zhang, C. Huang, Y. Huang, L. Tian, P. Wang, Z. Guo and Q. Jiang, *Adv. Compos. Hybrid Mater.*, 2023, **6**, 166.
- 44 Y. F. Chen, W. R. Chang, C. J. Lee and C. W. Chiu, *J. Mater. Chem. B*, 2022, **10**, 9974–9983.
- 45 J. W. Jeon, P. A. Ledin, J. A. Geldmeier, J. F. Ponder Jr, M. A. Mahmoud, M. El-Sayed, J. R. Reynolds and V. V. Tsukruk, *Chem. Mater.*, 2016, **28**, 2868–2881.
- 46 J. S. DuChene, W. Niu, J. M. Abendroth, Q. Sun, W. Zhao, F. Huo and W. D. Wei, *Chem. Mater.*, 2013, **25**, 1392–1399.
- 47 M. Thiele, J. Z. E. Soh, A. Knauer, D. Malsch, O. Stranik, R. Müller, A. Csáki, T. Henkel, J. M. Köhler and W. Fritzsche, *Chem. Eng. J.*, 2016, **288**, 432–440.
- 48 T. Y. Liu, J. Y. Ho, J. C. Wei, W. C. Cheng, I. H. Chen, J. Shiu, H. H. Wang, J. K. Wang, Y. L. Wang and J. J. Lin, *J. Mater. Chem. B*, 2014, **2**, 1136–1143.
- 49 A. K. Gaharwar, L. M. Cross, C. W. Peak, K. Gold, J. K. Carrow, A. Brokesh and K. A. Singh, *Adv. Mater.*, 2019, **31**, 1900332.
- 50 F. Persano, S. Batasheva, G. Fakhru'llina, G. Gigli, S. Leporatti and R. Fakhru'llin, *J. Mater. Chem. B*, 2021, **9**, 2756–2784.
- 51 T. A. König, P. A. Ledin, J. Kerszulis, M. A. Mahmoud, M. A. El-Sayed, J. R. Reynolds and V. V. Tsukruk, *ACS Nano*, 2014, **8**, 6182–6192.
- 52 J. W. Li, H. A. Tsai, H. T. Lee, Y. H. Cheng, C. W. Chiu and M. C. Suen, *Prog. Org. Coat.*, 2020, **145**, 105702.
- 53 W. R. Premasiri, Y. Gebregziabher and L. D. Ziegler, *Appl Spectrosc.*, 2011, **65**, 493–499.
- 54 W. R. Premasiri, J. C. Lee, A. Sauer-Budge, R. Théberge, C. E. Costello and L. D. Ziegler, *Anal Bioanal. Chem.*, 2016, **408**, 4631–4647.
- 55 W. R. Premasiri, Y. Chen, P. M. Williamson, D. C. Bandarage, C. Pyles and L. D. Ziegler, *Anal Bioanal. Chem.*, 2017, **409**, 3043–3054.
- 56 F. Hamadi and H. Latrache, *Colloids Surf. B*, 2008, **65**, 134–139.
- 57 J. Y. Ho, T. Y. Liu, J. C. Wei, J. K. Wang, Y. L. Wang, and J. J. Lin, *ACS Appl. Mater. Interfaces*, 2014, **6**, 1541–1549.
- 58 Y. Jing, R. Wang, Q. Wang, Z. Xiang, Z. Li, H. Gu and X. Wang, *Adv. Compos. Hybrid Mater.*, 2021, **4**, 885–905.

- 59 X. Yang, L. Sheng, Y. Ye, J. Sun, S. Geng, D. Ning, Y. Zhang and X. Sun, *Chem. Eng. J.*, 2023, **474**, 145771.
- 60 T. Wang, E. Fleming and Y. Luo, *Adv. Compos. Hybrid Mater.*, 2023, **6**, 6.
- 61 L. Zhao, G. Rosati, A. Piper, C. C. C. Silva, L. Hu, Q. Yang, F. D. Pelle, R. R. Alvarez-Diduk and A. Merkoçi, *ACS Appl. Mater. Interfaces*, 2023, **15**, 9024–9033.
- 62 [Y. Tan, Q. Yang, M. Zheng, M. T. Sarwar H. Yang, *Adv. Healthc. Mater.*, 2023, doi: 10.1002/adhm.202302700.](#)
- 62
- 63 [M. Long, Q. Liu, D. Wang, J. Wang, Y. Zhang, A. Tang, N. Liu, B. Bui, W. Chen and H. Yang, *Mater. Today Adv.*, 2021, **12**, 100190.](#)
- 63